Stationary localized structures and pulsing structures in a cavity soliton laser

P. Genevet, S. Barland, M. Giudici, and J. R. Tredicce
Université de Nice Sophia Antipolis, Institut Non-Linéaire de Nice, UMR 6618, 06560 Valbonne, France
(Received 12 December 2008; published 16 March 2009)

A cavity soliton laser is a device able to generate single-peak localized structures, also called cavity solitons, without the injection of an external coherent beam. We realized experimentally a cavity soliton laser by mutually coupling in face to face configuration two broad-area vertical cavity surface emitting lasers, one set to work as amplifier while the second, biased below transparency, plays the role of a saturable absorber. We explore the parameter space, showing the robustness of cavity solitons in this system, and we analyze their switching process. We also report on structures pulsing at the roundtrip time of the compound cavity defined by the two devices. Despite these structures look very similar to cavity solitons in terms of the time-averaged intensity profile, they cannot be interpreted as pulsing cavity solitons since there is no bistability associated with them.

DOI: 10.1103/PhysRevA.79.033819 PACS number(s): 42.65.Tg, 42.55.Px, 42.65.Pc

I. INTRODUCTION

Cavity solitons (CSs) are single-peak localized structures appearing in cavity filled with a nonlinear medium [1]. Since the 1990s, CSs have been actively investigated because of some of their properties that make them very promising for applications in all-optical information processing. They can be individually written and erased by shining (local) laser pulse inside the cavity, and their position can be controlled by introducing, along the resonator section, proper gradients in some parameter of the system [2,3]. Their potential in terms of applications is further enhanced when their plasticity is implemented in fast responding and small scale devices such as semiconductors microresonators [4]. The existence of CS in semiconductor resonators has been experimentally demonstrated in broad-area vertical cavity surface emitting lasers (VCSELs) used as amplifiers and injected by a coherent and homogeneous beam [holding beam (HB)] [5–7]. This configuration has been used as test bench for applications of CS to all-optical information processing. Several prototypical devices have been demonstrated such as a reconfigurable optical memory based on CS bits [8], an all-optical optical delay line [9], and a nondestructive probe of the semiconductor resonator defects [10]. Even if CSs are theoretically well understood, their application in nonprototypical devices remains difficult to implement due to the tight requirements on the parameters of the injected beam and on the degree of complexity of the experimental scheme.

A solution to these problems is provided by the cavity soliton laser (CSL), a device where CSs are self-generated without an external coherent injected beam. An important step in this direction have been recently accomplished with the realization of CSL based on broad-area VCSEL submitted to frequency-selective feedback [11]. Nevertheless, even if no HB is present, it appears that CS stability depends critically both on feedback alignment and on frequency tuning of the external grating. An alternative approach to the realization of CSL can be followed using lasers with saturable absorber (LSAs). LSAs have been used since a long time to generate high intensity pulses [12] and bistability [13]. A pioneering theoretical work have also shown that this system can be exploited, in the limit of fast material, for generating dissipative "autosolitons" [14]. This prediction was later extended to the case of finite relaxation times [15,16]. The situation of slow absorbing material was examined theoretically in [17], showing the existence of CS in LSA based on semiconductor materials. Finally, the case where the absorbing and gain media have equal response times has been studied in [18]. The authors of these last references show numerically that, in a VCSEL with saturable absorber, CS can be switched on and off by injecting a local optical perturbation.

In addition to be a candidate for the generation of stationary CS, LSA is also very interesting from the point of view of the formation of spatiotemporal solitons or light bullets [19,20]. Light bullets are pulses of light not spreading neither in time nor in space, i.e., tridimensional localized structures. In a nonlinear optical resonator a bidimensional pulsing CS can be considered as a light bullet provided that the pulse duration is much shorter than the cavity round-trip time. Though widely investigated, we are not aware of any experimental observation of these structures, neither in the frame of pattern forming systems nor in the frame of nonlinear waveguide. From the experimental point of view, a CSL based on SA has been recently realized using two nominally identical broad-area VCSELs facing each other [21]. One of the two VCSELs is used in the amplifying regime while the second is kept below the transparency, thus playing the role of a saturable absorber. This work paves the way toward a miniaturized version, which would include both coupled cavities in a single monolithic broad-area device [22–24].

In this paper, we present an extensive experimental analysis of the stationary CS obtained using this configuration. After the description of the experimental setup (Sec. I), we analyze the CS stability in the parameter space (Sec. II). We show the transverse patterns appearing in the system and their connection with CS (Sec. III). We study the possibility of switching CS by shining a laser pulse into the compound system and the CS switching dynamics (Sec. IV). We also report on the existence of nonstationary single-peak structures which bifurcate from stationary CS (Sec. V). While the time-averaged intensity profile of this structure is very similar to the CS profile, we show that they do not coexist with

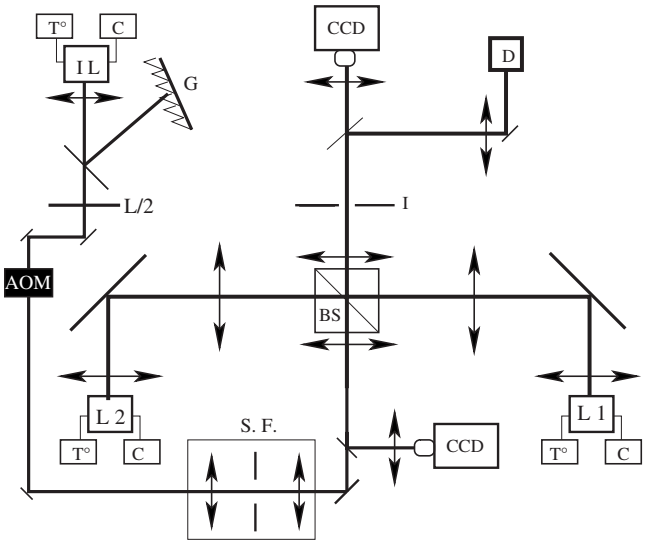

FIG. 1. Schematic of the experiment. L1, laser above the transparency; L2, laser below the transparency; IL, incoherent writing laser; bs, beam splitter; D, high-bandwidth detector; CCD, charge-coupled device camera; T°, temperature controller; C, power supply; $L/2$, half-wave plate; G, grating; AOM, acousto-optic modulator; S.F., spatial filter; and I, iris.

any other structure nor with an homogeneous state. Absence of bistability discards the possibility of interpreting them as pulsing CS.

II. EXPERIMENTAL SETUP

The experimental setup is presented in Fig. 1. Two nominally identical VCSELs L_1 and L_2 are mounted in face to face configuration at a distance $d=60$ cm. They are 200 μm diameter disklike lasers. The near field output of L_1 is imaged onto the near field output of L_2 and vice versa. The two VCSELs, inside which diffraction takes place, hence delimit a self-imaging cavity whose round-trip time τ_c is approximately 4 ns. In this configuration, L_1 and L_2 are placed in self-conjugate planes and therefore, after one round-trip, L_1 (L_2) is re-imaged on itself. This configuration allows to compensate for the diffraction occurring between the two VCSELs, hence preserving the high Fresnel number required for the existence of LS [1]. A 20% reflection beam splitter is inserted in the center of the cavity to extract output beams from the compound system. We underline that the results presented in this paper could not be obtained using a 50% reflection beam splitter, indicating that the amount of coupling between the devices must be sufficiently high. The near-field profiles of each VCSEL are imaged on two charge-coupled device (CCD) cameras, allowing the simultaneous monitoring of L_1 and L_2. The self-imaging condition is obtained experimentally by comparing onto a single CCD camera the image of the near-field-emission profile of L_2 with the near-field-emission profile of L_1 reflected by the resonator surface of L_2 (the two resonators being uncoupled due to large temperature-induced detuning between the resonators, as described in Sec. III). If, after reflection, L_1 profile is also imaged onto the CCD camera and this image has the same size as the near field image of L_2, then self-imaging condition is reached. (Fig. 2).

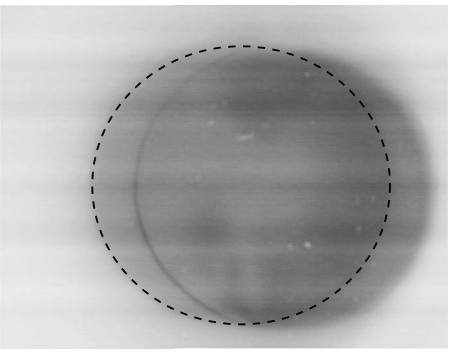

FIG. 2. Near-field (NF) emissions of L_1 and L_2 when the self-imaging condition is reached (dark areas correspond to high intensities). The left circle corresponds to the NF of laser L_1 imaged on the laser L_2 (right circle) and reflected by the exit mirror of L_2 when the two resonators are not coupled (large cavity resonances detuning due to large temperature induced detuning, see Sec. III). The right circle is the image of the NF profile of L_2. The same result can be found inverting the role of the resonators and imaging directly L_1. Both VCSELs are biased at few mA.

L_1 and L_2 are two broad-area VCSELs emitting at 980 nm, produced by ULM photonics. They come from the same wafer and they are nominally identical, their standalone threshold is about 400 mA. Their substrate temperatures (T_1° and T_2°) and pumping currents (J_1 and J_2) are stabilized. Since L_1 is used in the amplifying configuration, while L_2 is used in absorbing configuration, L_1 is biased at current values larger than L_2. The index of refraction of the semiconductor medium depends both on substrate temperature and on pumping current through Joule heating. The mismatch between the cavity resonances, implied by a difference in the bias currents, can be therefore compensated by controlling the individual substrate temperatures (T_1° and T_2°), thus enabling coupling between the two resonators. The coupling level between the two resonators depends also on the reflectivity of the beam splitter inserted in the cavity for extracting output beams. In order to maximize the coupling, we choose the minimal reflectivity still enabling extraction of detectable output beams. High-bandwidth detection of a small area of the near-field profile is obtained by placing an iris on the detection path and monitoring the transmitted output with a fast photodetector Thorlabs PDA865 (50 ps rise time) coupled to a digital Lecroy Wavemaster 8600A (6 GHz analog bandwidth). In order to ignite CS we used a 15 μm size writing beam (WB) generated by an external-cavity tunable laser mounted in Littman configuration. The WB is applied to a point of the transverse profile of the absorbing resonator (L_2) acting as a local optical perturbation of the compound system. An acousto-optic modulator allows for switching on and off the writing beam.

III. PARAMETER SPACE

CS existence relies on the presence of a bistable emission of the system [1]. In this section, we explore the existence of

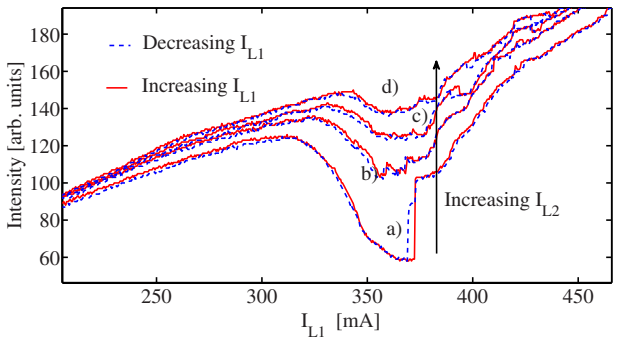

FIG. 3. (Color online) Local intensity output emitted by the system when scanning I_{L1} with a fixed difference of packages temperature $\Delta T^{\circ}=-9.2$ °C for different values of I_{L2}. The continuous curves correspond to an increase in I_{L1} while the dashed part of the curves corresponds to a decrease in I_{L1}. Curve (a) corresponds to a value of $I_{L2}=16$ mA, curve (b) $I_{L2}=30$ mA, curve (c) $I_{L2}=38$ mA, and curve (d) $I_{L2}=46$ mA. For sufficiently low values of I_{L2} a bistable cycle appears. The monitored region has a diameter of about 15 μm and it is placed close to the center of L_1, see Fig. 5.

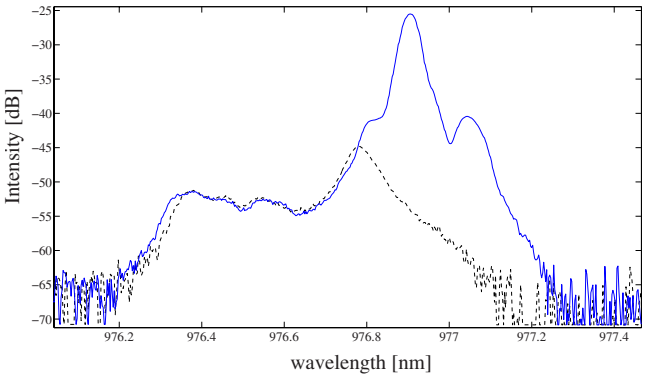

FIG. 4. (Color online) Optical spectrum of the system output monitored locally as in Fig. 3, curve (a). Dashed line: optical spectrum corresponding to the low state emission of bistability curve (a) shown in Fig. 3. Continuous line: optical spectrum corresponding to the upper state of bistability curve (a) of Fig. 3. We notice that 60 arb. units correspond to the spontaneous emission level.

bistability in the parameter space. As explained above, the detuning between the resonant frequencies of the two VCSELs resonators $\theta=\omega_{c,L_1}-\omega_{c,L_2}$ depends both on the substrates temperatures (T_1° and T_2°) of the two devices and on their bias currents (I_{L1} and I_{L2}). In Fig. 3, we show the local intensity output emitted by the system when scanning I_{L1}. As initial setting [curve (a) in Fig. 3] we choose $\Delta T^{\circ}=T_1^{\circ}-T_2^{\circ}=-9.2$ °C and $I_{L2}=16$ mA. For $I_{L1}=0$ mA we have a finite negative value for θ due to the difference between the substrate temperatures and the bias currents. As I_{L1} is increased the cavity resonance of L_1 is red shifted due to Joule heating of semiconductor medium and θ increases toward zero.

For $I_{L1}<110$ mA, the compound system is below threshold since no coherent emission is detected by an optical spectrum analyzer. When $I_{L1}\sim 110$ mA the system reaches its compound threshold. Because of the large value of θ, L_1 and L_2 are not interacting and L_2 output mirror is reflecting back the light emitted by L_1. In this regime the system is analogous to a laser with an external mirror [25] and the value at which I_{L1} reaches the compound threshold does not depend on the parameter setting of L_2. For $I_{L1}\sim 320$ mA, $|\theta|$ is small enough such that the two resonators may interact. As I_{L1} is increased, $|\theta|$ further decreases and we observe a progressive drop in the output level as a consequence of an increasing absorption by L_2, reducing the amount of light fed back to L_1. For $I_{L1}\sim 370$ mA, $|\theta|\approx 0$ and the intensity output reaches the lowest level, if L_2 is unpumped, the measured photocurrent in I_{L2} reaches the value of 35 mA. The optical spectra of this low intensity regime (see Fig. 4, dashed line) shows a broad band peak, indicating that this state corresponds to spontaneous emission and confirming that absorption from L_2 has suppressed the feedback mechanism for L_1.

Further increase in I_{L1} above a critical value I_{L1}^{c} determines a sudden jump of the intensity output to a high value. The optical spectrum associated to this state shows a well-pronounced peak red-detuned with respect to the spontaneous emission peak observed in the low level state (see Fig. 4). This coherent emission can be interpreted by a local lasing action of the compound system appearing subcritically due to the saturation of the absorption in L_2. After this phase transition, if I_{L1} is decreased, the intensity output shows hysteresis indicating the presence of bistability between a low and a high emitted intensity states in the region monitored by the detector. This interpretation can be confirmed by short circuiting L_2, such that the absorption has an effectively infinitely fast relaxation. In this case L_2 it is not saturable anymore and no bistability is observed although a light-induced current can be detected in L_2.

The local jump to the high-level intensity output state corresponds, in the near-field profile, to the formation of a bright single-peak structure inside the monitored area, as shown in Fig. 5. Together with the monitored spot, we notice that also other single-peak structures has appeared in the transverse section as I_{L1} has been increased. Though these structures appears also subcritically with a homogeneous low-intensity state, it is important to notice that they are not appearing exactly for the same critical value of I_{L1}. As al-

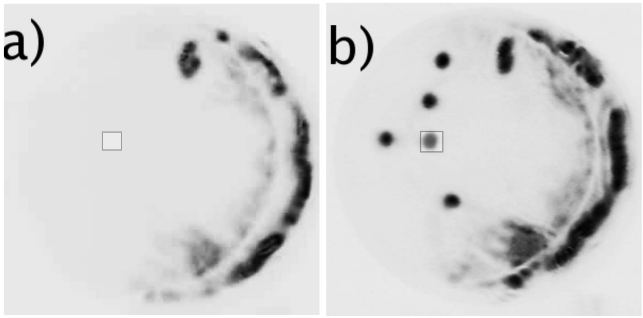

FIG. 5. Left panel: Near-field intensity profile when the system is locally in the low-level emission state of Fig. 3, curve (a). Right panel: near-field intensity profile when the system is locally at the high-level intensity state of Fig. 3, curve (a). Dark areas correspond to high intensities. The position of the local area monitored in Fig. 3 is indicated by the square. The near-field profile shown is obtained from L_1, the same profile is observed monitoring L_2 [21]. The diameter of the observed structures is about 10 μm.

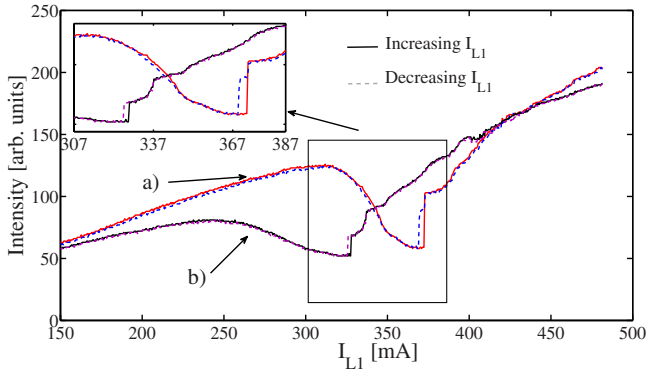

FIG. 6. (Color online) Local intensity emitted by the system as a function of I_{L1}, for two different temperature stabilization settings (ΔT°). The continuous curve is obtained by increasing I_{L1} while the dashed part of the curve is obtained by decreasing I_{L1}. In curve (a) $T_2^{\circ}=28.0\ ^{\circ}\mathrm{C}$, $I_{L2}=16.5$ mA, and $\Delta T^{\circ}=-9.2\ ^{\circ}\mathrm{C}$. In curve (b) $I_{L2}=7$ mA and $\Delta T^{\circ}=-7.5\ ^{\circ}\mathrm{C}$.

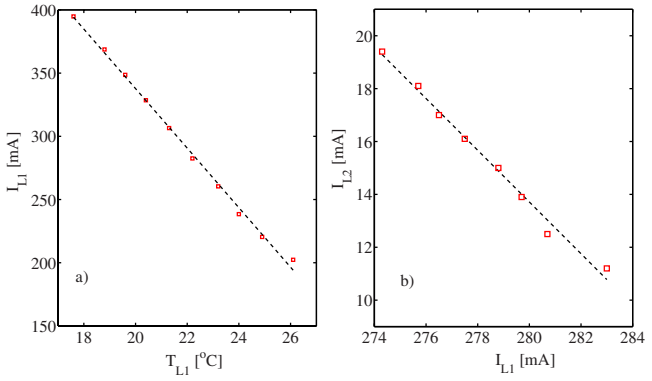

FIG. 7. (Color online) Left panel: I_{L1} value as a function of T_1° in order to observe the bistable behavior. $I_{L2}=10$ mA, $T_2^{\circ}=28.9\ ^{\circ}\mathrm{C}$. Right panel: I_{L2} value as a function of I_{L1} in order to obtain bistability. $T_1^{\circ}=22.4\ ^{\circ}\mathrm{C}$, $T_2^{\circ}=28.9\ ^{\circ}\mathrm{C}$. Dashed lines indicates linear fits.

ready noted in previous experiments on CS [7,8], surface roughness of the optical resonator induces fluctuations of parameter θ throughout the transverse dimension of the VCSELs and, as a consequence, the single-peak structures appear spontaneously for slightly different values of parameters. The single-peak structures shown are candidate for being cavity solitons since they appear subcritically coexisting with homogeneous background. This interpretation have been validated through individual addressing by a local beam (writing beam). This operation is described in Sec. V and in [21]. For larger I_{L1} the local intensity keeps increasing, while the near field reveals the formation of complex extended nonstationary patterns that will be described in Sec. IV.

When the two devices are interacting, the amount of light fed back to L_1 (or, equivalently, the amount of light absorbed by L_2) can be varied by changing I_{L2}. This is shown in Fig. 3, where, in addition to curve (a) described above, we also plot two scans of I_{L1} for different values of I_{L2}. When I_{L2} is increased, the level of absorption is decreased, the intensity drop is less pronounced, and the bistability cycle tends to disappear [curve (b) in Fig. 3]. As I_{L2} is increased approaching the transparency value, the bistability cycle disappears completely [curves (c) and (d)] and further increase in I_{L2} also makes the drop of intensity output vanish.

In Fig. 6, we show the local intensity output curve as a function of I_{LI} for different settings of the substrates temperatures T_1°, T_2°, and I_{L2}. The interaction region and the bistable cycle occur at different values of I_{L1}. ΔT° must be negative in order to compensate for the different bias current of the two devices (see curve for $\Delta T=-9.2\ ^{\circ}\mathrm{C}$ with $I_{L2}=16.5$ mA). An increase in this parameter makes the bistability region get closer to the compound system threshold (see curve for $\Delta T=-7.5\ ^{\circ}\mathrm{C}$, $I_{L2}=7$ mA). In these conditions the drop gets smoother and the bistability region shrinks.

Interestingly, for this setting, the presence of plateaux in the local intensity output curve beyond the bistability cycle is associated to appearance of multipeaks structures in the near-field profile. These multipeaks structures can also be bistable depending on parameters. The analysis of these complexes is beyond the scope of this manuscript and it will be presented elsewhere.

In Fig. 7 we locate the bistability region as a function of I_{L1} and T_1° once fixed I_{L2} and T_2°. The linear dependence obtained indicates the possibility of varying I_{L1} and T_1° in order to set suitable tuning between the two cavity resonances allowing for bistability. The curve slope results from the ratio between the (linear) dependencies of the wavelength of the cavity resonance (λ_c) with respect to the pumping current and the substrate temperature of the device $\frac{\partial \lambda_c}{\partial I_{L1}}$, $\frac{\partial \lambda_c}{\partial T_1^{\circ}}$. This slope indicates that it is necessary to decrease the laser current of 23.5 mA for every degree of increase in the substrate temperature in order to maintain λ_c unchanged. The individual dependencies are measured individually and they are $\frac{\partial \lambda_c}{\partial I_{L1}}=0.005$ nm/mA and $\frac{\partial \lambda_c}{\partial T_1^{\circ}}=0.114$ nm/°C. We conclude that the bistability region can be found on a large set of different pairs of values (T_1°, I_{L1}), which all correspond to equivalent tuning conditions between both devices.

Around the parameters values shown in Fig. 7 [panel (a)], the bistable domain exists over a narrow range of detuning values (θ) between the two resonances (approximately 0.05 nm, i.e., 15 GHz), while interaction between the two resonators can be estimated from Fig. 3 to occur up to few angstroms detuning between the two resonances, due to the finite width of the cavities resonances. Within this large tuning condition for interaction, fine adjustment of the bias currents allows for controlling bistability. This is shown in Fig. 7 (right panel) where we draw the location of bistability (using as reference I_{L1}^c) versus the current of the two devices, when both devices packages temperatures are fixed. Bistability domain as a function of the two bias currents I_{L2} and I_{L1} shows a slope of -1, indicating that somehow a larger absorption rate (decrease in I_{L2}) must be compensated by a larger gain (increase in I_{L1}) in order to maintain bistability. It is not surprising that the dependence of gain on I_{L1} and absorption on I_{L2} is the same since the two devices are nominally identical. It is worth to point out that this compensation in terms of bias currents pulls the two cavities resonance in opposite directions, and therefore it is possible only in a limited range of currents (10 mA), otherwise the proper tuning condition is lost. This behavior gives some freedom on the ratio between amplification and absorption in the system resulting in a bistable behavior. The effect of this parameter on the struc-

tures appearing in the system will be presented elsewhere.

To conclude this section, we underline that the bistability cycle can be found in a broad region of parameter space, as long as certain conditions are satisfied. The large number of tunable parameters allows for setting the system in a bistable behavior on a large set of parameters. Two main criteria must be fulfilled anyhow: I_{L2} must be lower than transparency (in our system $I_{L2}<35$ mA) and the temperature difference of the substrates (ΔT°) must be sufficiently negative ($T_1^{\circ}<T_2^{\circ}$) such that the matching condition between the two cavities ($\theta\approx 0$) must occur for I_{L1} larger than the compound system threshold. This threshold, which depends on the feedback from the facet of L_2, can be decreased by lowering the reflectivity of the intracavity beam splitter.

IV. PATTERN FORMATION

As shown in the preceding section, formation of spatially extended patterns in the near-field-emission profile of the system occurs when I_{L1} is increased well above I_{L1}^c. In the self-imaging condition the output profile of L_1 is imaged on L_2 and vice versa (as shown in Fig. 2). As a consequence, when both systems are interacting, the spatial structures present in the transverse section of each device are identical (see [21]). In Fig. 8 we show the typical behavior of the system when the current of L_1 is increased, starting from the upper branch of the bistable region [panel (a)] until the pattern is completely developed [panel (h)]. In Fig. 8(a) we observe five distinct isolated spots from which, as I_{L1} is increased, filaments of light develop. This is observed in Fig. 8(b), where several filaments appear connecting the solitary spots with the neighboring extended structures. The fast temporal detection reveals a complex pulsating behavior along these filamented structures. Moreover, in the top part of the near-field profile, a single spot becomes a stationary three peaks structure [panel (b)]. Upon further increase in I_{L1}, the extended patterns develop from these initial spots. The complex temporal behavior persists even when a whole pattern is developed. The spatial shape of the time-averaged intensity of these patterns strongly differ from the stationary patterns formed in driven semiconductor lasers [26,27]. Indeed, these previous experiments presented well-structured patterns, such as stripes or hexagons, while the ones observed here look more like domains. Theoretical investigation are in progress in order to disclose the nature of the observed structures.

V. INCOHERENT ADDRESSING OF CS

In injected systems CS can be easily switched on and off by using a local perturbation in form of a narrow beam in phase or out of phase with the driving field [5,7]. This procedure is not possible in a cavity soliton laser because of the absence of a driving field, i.e., a holding beam that would lock the phase of the system. In [28], the authors considered different switching methods in a CSL. They showed that the most efficient method in a CSL based on a saturable absorber is to inject an incoherent laser beam, tuned at the frequency of the cavity soliton. CS control is achieved by shining light

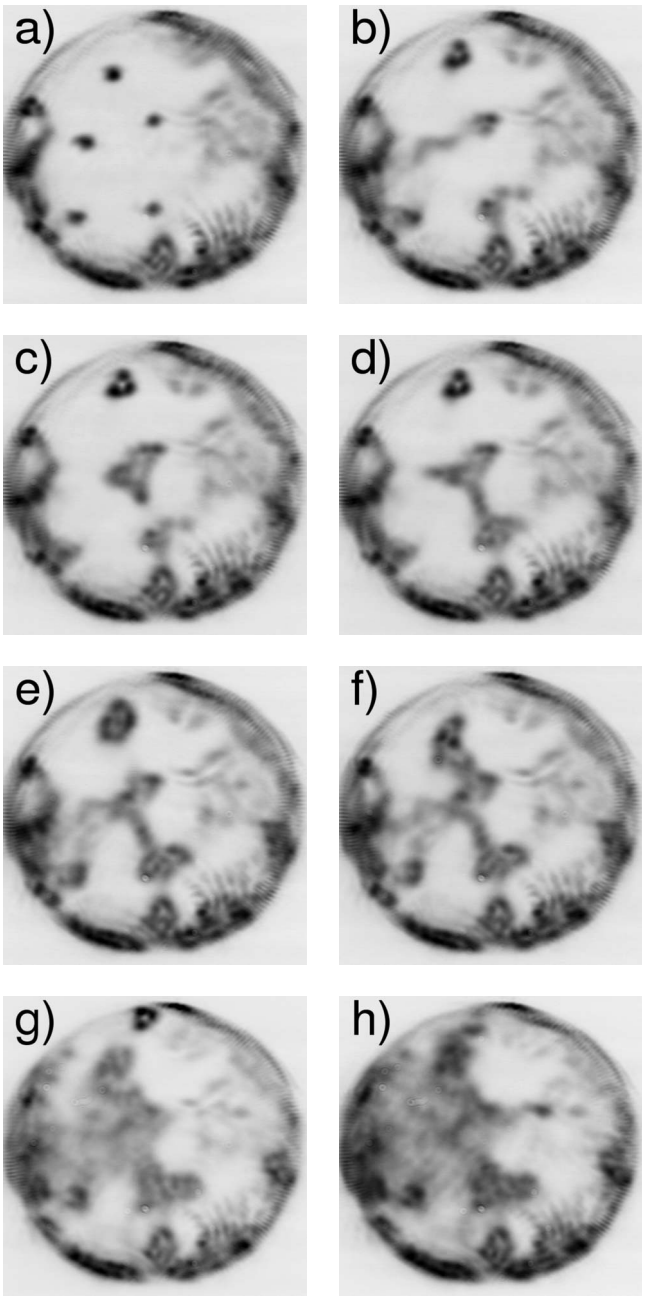

FIG. 8. Sequence showing the patterns forming beyond the bistable zone. From (a) to (h), only I_{L1} is increased. (a) $I_{L1}=408.5$ mA, (b) $I_{L1}=419.7$ mA, (c) $I_{L1}=419.8$ mA, (d) $I_{L1}=421.5$ mA, (e) $I_{L1}=428.6$ mA, (f) $I_{L1}=430.2$ mA, (g) $I_{L1}=445$ mA, (h) $I_{L1}=453$ mA. All the other parameters constant: $I_{L2}=2.2$ mA, $T_1^{\circ}=18.0$ °C, and $T_2^{\circ}=28.9$ °C.

pulses into the cavity; it turns out that writing operation and erasing operation requires different WB pulse duration. In order to control the CS state in our system we apply the same procedure. An external-cavity laser emits a beam of approximately 15 μm diameter, and it is tuned close to the emission wavelength of the cavity soliton (within 0.1 nm precision). This beam passes through an acousto-optic modulator that enables intensity control of the beam (Fig. 1). The beam is used to target a point in the transverse section of the absorber, acting as an external incoherent optical perturbation,

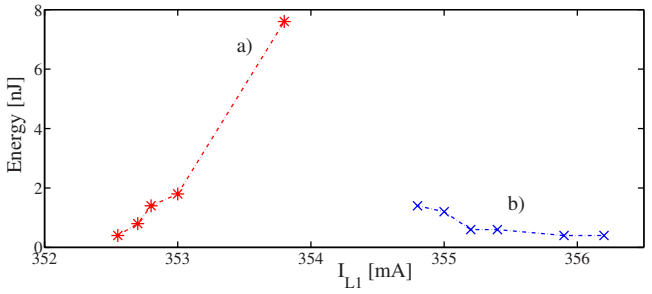

FIG. 9. (Color online) Writing beam pulse energy necessary to switch on [curve (a)] and off [curve (b)] a CS as a function of I_{L1}. The structure is bistable between 352.4 and 356.4 mA. The required pulse duration decreases as the parameter is set closer to the edges of the bistable cycle. I_{L2}=9.1 mA and ΔT°=−9 °C.

i.e., as a incoherent WB. CS ignition has been reported in [21], showing addressing of two independent single-peak CSs which are 10 μm broad. We point out that, as in previous experiments in semiconductor devices [7,11], local inhomogeneities of the device affect the possibility of creating localized structures at arbitrary positions for the same set of parameters. In Fig. 9 we plot the energy of the WB pulse needed to switch on and off the cavity soliton as a function of I_{L1}. The WB square pulse energy was varied by changing the pulse duration, being 2 mW pulse power amplitude. The targeted CS is bistable between 352.4 and 356.4 mA. We remark that the WB energy required to address the CS decreases as I_{L1} approaches the edges of the bistability region. In the experimental setup we used it was not possible to find values of I_{L1} such that we could switch on and off a cavity soliton by varying only the pulse duration, as shown numerically in [28]. This is evidenced in Fig. 9 where we show that the curves for WB pulse energy for switching on and off operations does not share any I_{L1} values. Superposition of the two curves might be reached by increasing the WB power, this was not possible in our setup due to the power limitation of the WB. In order to enable CS switching off without changing I_{L1}, we take advantage of the mobility of CS together with the existence of region in the transverse section of the device where CSs are not stable. CSs easily couple to any perturbation of the translational symmetry and therefore they drift transversely along a parameter gradient. A constant WB applied to a point of the transverse section is a trapping intensity gradient for the CS and it can be used to drag them toward the regions where CSs are unstable. In this way CS can be switched off [21].

In the bistable region, a mechanical perturbation, such as a little knock on the optical table, is capable of switching on a CS. In Fig. 10 we show the switching process. CS switching process exhibits a long-lasting (around 600 ns) oscillatory transient. This transient is characterized by pulses at the round-trip time of the external cavity ($\tau_c \sim 4$ ns) with a duration of around 150 ps. The same transient dynamics is observed when a CS is switched on by using a WB pulse perturbation.

VI. NONSTATIONARY STRUCTURES

One of our motivation in exploring CSL based on saturable absorber is the possibility of creating light bullets, i.e.,

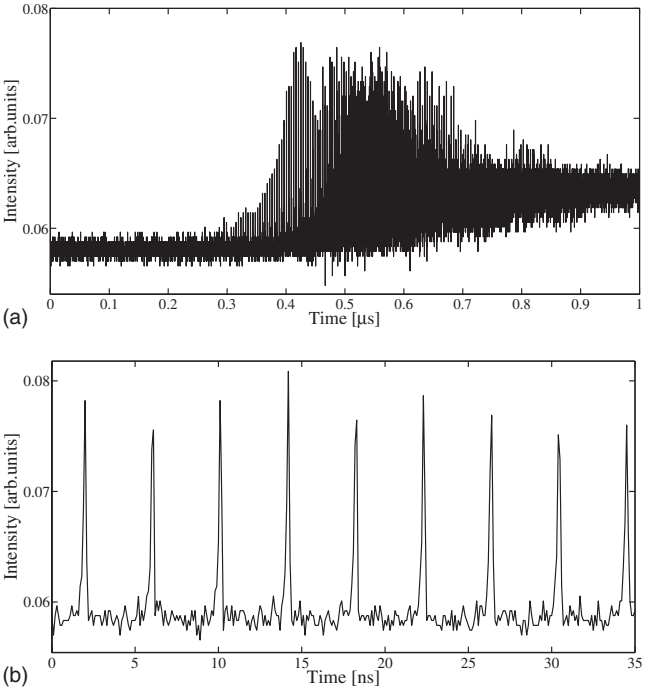

FIG. 10. (a) Switching transient of a CS when applying a mechanical perturbation. I_{L1}=278.8 mA, I_{L2}=15 mA, and ΔT°=−6.8 °C. (b) Zoom of the transient.

localized states of light both in time and space. For this reason, we build on the existence of two-dimensional (2D) localized structures and we try to set proper conditions in order to get these localized structures pulsing. In particular, narrow pulses at the round-trip frequency of the cavity have been obtained in mode-locked vertical external-cavity surface emitting laser (VECSEL) with saturable absorber or reverse bias quantum well device as external mirror [12,29]. When the cavity round-trip time is exceedingly large with respect to the carrier recombination rate, multiple-pulse regime takes place affecting the stability of single pulse mode locking [12]. For this reason we decrease the distance between L_1 and L_2 down to d=6 cm, which is the minimum distance we can achieve still inserting the laser collimators and the output beam splitter between the two devices. The two lenses placed in between the two lasers are removed and self-imaging condition is obtained by setting the position of the collimators. Stationary CSs are obtained, as previously described for d =60 cm when $I_{L2}<35$ mA. Their existence in parameter space is equivalent to the one described in Sec. III. This is not surprising since the self-imaging condition is maintained and therefore d is not a relevant parameter for diffraction. Increasing I_{L1} above the bistable range, CSs evolve toward structures that are not bistable anymore and, in particular, they cannot be switched off by a WB. It is important to point out that the time-averaged intensity profile of the CS does not show appreciable changes when they evolve toward monostable structures. While in the bistable regime CSs were stationary, the monostable structures can be pulsing. This is shown in Fig. 11, where we show the temporal behavior of one of these structures for I_{L1} above the bistability region. The structure monitored is indicated by an arrow in

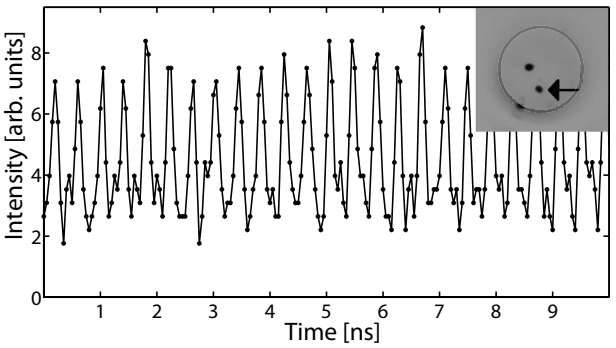

FIG. 11. Typical temporal behavior of an isolated structure bifurcating from CS but not anymore bistable. The inset picture shows the associated near-field-emission profile. The arrow indicates the monitored pulsing spot. $I_{L1}=266.3$ mA, and $I_{L2}=25.3$ mA.

the near-field profile of L_1 (see inset of Fig. 11) and the same isolated spot becomes a cavity soliton for slightly lower value of I_{L1}. The pulsing of the monostable structure occurs at $2d/c=0.4$ ns, i.e., at the round-trip time of the cavity defined by the two devices. The pulse width is shorter than 150 ps, being the pulse detection limited by the oscilloscope bandwidth. Despite the similarity in terms of the profile, it is clear that this pulsing structure cannot be claimed to be a pulsing localized structure since no bistability is associated with it.

VII. CONCLUSION

Cavity solitons laser is a device able to generate CS without injection of any coherent holding beam. We have analyzed experimentally the possibility of building this device by using two broad-area VCSELs in self-imaging face to face configuration. Stationary CSs exist when one of the two devices is biased below transparency playing the role of a saturable absorber. We have analyzed the parameter space region where CSs are stable, and we have shown that stability can be obtained by proper tuning of the control parameters on a wide range. We have analyzed the energy requirement for CS addressing and the transient switching behavior. We have shown that, beyond the bistability region, nonstationary extended pattern develops. On the other hand, vertical external-cavity semiconductor lasers with saturable absorber as external mirror and forced single transverse-mode operation are widely used schemes to generate ultrashort and periodic pulses. The possibility of implementing this functionality in broad-area devices is extremely interesting in view of achieving three-dimensional localization of light. We have shown the existence of monostable structures with a transverse profile very similar to the cavity solitons pulsing at the round trip of the external cavity. Despite these characteristics, this single spot structure cannot be claimed to be a light bullet since no bistability is associated with it and therefore its independence from the rest of the system cannot be demonstrated.

ACKNOWLEDGMENTS

This work was supported by the FET Open Project FunFACS (www.funfacs.org). The authors would like to thank L. Gil and L. Columbo for many useful discussions.

[1] L. A. Lugiato, IEEE J. Quantum Electron. **39**, 193 (2003), and references therein.
[2] M. Brambilla, L. A. Lugiato, and M. Stefani, Europhys. Lett. **34**, 109 (1996).
[3] W. J. Firth and A. J. Scroggie, Phys. Rev. Lett. **76**, 1623 (1996).
[4] M. Brambilla, L. A. Lugiato, F. Prati, L. Spinelli, and W. J. Firth, Phys. Rev. Lett. **79**, 2042 (1997).
[5] S. Barland, J. R. Tredicce, M. Brambilla, L. A. Lugiato, S. Balle, M. Giudici, T. Maggipinto, L. Spinelli, G. Tissoni, T. Knödlk, M. Millerk, and R. Jäger, Nature (London) **419**, 699 (2002).
[6] *Dissipative Solitons: From Optics to Biology and Medicine Series*, edited by N. Akhmediev and A. Ankiewicz, Lecture Notes in Physics Vol. 751 (Springer, Berlin, 2008).
[7] X. Hachair, S. Barland, L. Furfaro, M. Giudici, S. Balle, J. R. Tredicce, M. Brambilla, T. Maggipinto, I. M. Perrini, G. Tissoni, and L. Lugiato, Phys. Rev. A **69**, 043817 (2004).
[8] F. Pedaci, P. Genevet, S. Barland, M. Giudici, and J. R. Tredicce, Appl. Phys. Lett. **89**, 221111 (2006).
[9] F. Pedaci, S. Barland, E. Caboche, P. Genevet, M. Giudici, J. R. Tredicce, T. Ackemann, A. J. Scroggie, W. J. Firth, G.-L. Oppo, G. Tissoni, and R. Jäger, Appl. Phys. Lett. **92**, 011101 (2008).
[10] F. Pedaci, G. Tissoni, S. Barland, M. Giudici, and J. Tredicce, Appl. Phys. Lett. **93**, 111104 (2008).
[11] Y. Tanguy, T. Ackemann, W. J. Firth, and R. Jäger, Phys. Rev. Lett. **100**, 013907 (2008).
[12] U. Keller and Anne C. Tropper, Phys. Rep. **429**, 67 (2006).
[13] L. A. Lugiato, P. Mandel, S. T. Dembinski, and A. Kossakowski, Phys. Rev. A **18**, 238 (1978).
[14] N. N. Rosanov and S. V. Fedorov, Opt. Spectrosc. **72**, 782 (1992).
[15] S. V. Fedorov, A. G. Vladimirov, G. V. Khodova, and N. N. Rosanov, Phys. Rev. E **61**, 5814 (2000).
[16] N. N. Rosanov, *Spatial Hysteresis and Optical Patterns* (Springer, Berlin, 2002), Chap. 6.
[17] M. Bache, F. Prati, G. Tissoni, R. Kheradmand, L. A. Lugiato, I. Protsenko, and M. Brambilla, Appl. Phys. B: Lasers Opt. **81**, 913 (2005).
[18] F. Prati, P. Caccia, G. Tissoni, L. A. Lugiato, K. Mahmoud Aghdami, and H. Tajalli, Appl. Phys. B: Lasers Opt. **88**, 405 (2007).
[19] F. Wise and P. Di Trapani, Opt. Photonics News **13**, 26 (2002), and references therein.
[20] A. G. Vladimirov, S. V. Fedorov, N. A. Kaliteevskii, G. V. Khodova, and N. N. Rosanov, J. Opt. B: Quantum Semiclassical Opt. **1**, 101 (1999).

[21] P. Genevet, S. Barland, M. Giudici, and J. R. Tredicce, Phys. Rev. Lett. **101**, 123905 (2008).
[22] S. F. Lim, J. A. Hudgings, G. S. Li, W. Yuen, K. Y. Lau, and C. J. Chang-Hasnain, Electron. Lett. **33**, 1708 (1997).
[23] J. A. Hudgings, Robert J. Stone, Sui F. Lim, Gabriel S. Li, Wupen Yuen, Kam Y. Lau, and Connie J. Chang-Hasnain, Appl. Phys. Lett. **73**, 1796 (1998).
[24] A. J. Fischer, K. D. Choquette, W. W. Chow, H. Q. Hou, and K. M. Geib, Appl. Phys. Lett. **75**, 3020 (1999).
[25] J. H. Osmudsen and N. Gade, IEEE J. Quantum Electron. **19**, 465 (1983).
[26] Y. Menesguen, S. Barbay, X. Hachair, L. Leroy, I. Sagnes, and R. Kuszelewicz, Phys. Rev. A **74**, 023818 (2006).
[27] T. Ackemann, S. Barland, J. R. Tredicce, M. Cara, S. Balle, R. Jäger, M. Grabherr, M. Miller, and K. J. Ebeling, Opt. Lett. **25**, 814 (2000).
[28] K. Mahmoud Aghdami, F. Prati, P. Caccia, G. Tissoni, L. A. Lugiato, R. Kheradmand and H. Tajalli, Eur. Phys. J. D **47**, 447 (2008).
[29] K. Jasim, Q. Zhang, A. V. Nurmikko, E. Ippen, A. Mooradian, G. Carey, and W. Ha, Electron. Lett. **40**, 34 (2004).